

Ferroelastic phase transition and phonons in a diatomic-molecular monolayer

S. Y. Tang

Department of Physics, University of California, San Diego, La Jolla, California 92093

W. Jin and S. D. Mahanti

Department of Physics and Astronomy and Center for Fundamental Materials Research, Michigan State University, East Lansing, Michigan 48824-1116

R. K. Kalia

Argonne National Laboratory, Argonne, Illinois 60439-4843

(Received 26 May 1988)

Using a constant-pressure molecular-dynamics simulation, we have investigated the thermodynamics and the dynamics of a two-dimensional diatomic-molecular monolayer undergoing a ferroelastic phase transition. This system closely resembles the δ phase of oxygen molecules adsorbed on a graphite surface. For Lennard-Jones parameters appropriate for the oxygen molecules, we find a first-order transition from an orientationally ordered distorted triangular structure (ferroelastic phase) to an orientationally disordered equilateral triangular structure (paraelastic phase). The transition temperature is 20.1 K compared with 26 K for oxygen on graphite [coverage ≈ 8 molecules (100 \AA^2)] and the entropy associated with this transition is $0.88k_B$. The orientational diffusion constant increases by a factor of 30 at the transition. In addition, there is a strong softening of the elastic constants near the transition, particularly in the paraelastic phase; this can be understood in terms of translation-rotation coupling. Comparison between phonon frequencies for certain symmetry directions obtained by using quasiharmonic approximation and molecular-dynamics simulation clearly shows the presence of large anharmonicity effects in the paraelastic phase. A rapid quench from the high-temperature phase to very low temperatures indicates the presence of small clusters (consisting of 6–12 molecules) with both ferroelastic and herringbone ordering. In addition, we find a large density of equilateral triangular plaquettes. These give rise to a three-peak structure in the center-of-mass radial distribution function.

I. INTRODUCTION

Structural phase transitions (SPT's) and dynamics of three-dimensional (3D) molecular solids have been widely studied.¹ Typical systems are solid nitrogen (N_2),² solid oxygen (O_2),³ alkali cyanides (CN^-),⁴ alkali superoxides (O_2^-),⁵ and alkali nitrates (NO_2^-).⁶ These systems generally exhibit SPT's in conjunction with orientational order-disorder transitions where both translational and rotational degrees of freedom are involved.⁷ The SPT's associated with elastic (strain) deformation are called ferroelastic.⁸ For example, in three-dimensional KCN, at low temperatures, the solid has an orthorhombic structure in which all the CN^- molecules are oriented in one direction. When temperature is raised, it transforms into a cubic structure in which the CN^- molecules are orientationally disordered.⁹

A molecular overlayer adsorbed on a smooth crystalline surface can form a two-dimensional (2D) molecular solid. Molecular nitrogen (N_2) or oxygen (O_2) physisorbed on graphite surface serve as typical examples of such a 2D system.¹⁰ One of the important characteristics of molecular solids is the competition between direct and indirect (lattice mediated) intermolecular interactions which leads to different types of orientational order-

ing.^{11,12} Since the effect of this competition is pronounced in two dimensions due to enhanced fluctuations,¹³ one may see multiple stage phase transitions¹⁴ and in some cases, fluctuation-driven first-order phase transition.¹⁵

Physisorbed oxygen molecule on graphite exhibits a number of different phases depending on the coverage and temperature.¹⁶ There are extensive experimental investigations of this system. X-ray diffraction,¹⁷ magnetic susceptibility,¹⁸ heat capacity,¹⁹ neutron diffraction,²⁰ and low-energy electron diffraction²¹ (LEED) measurements have discovered a diverse phase structure. In particular, there is a low-coverage low-temperature phase (δ phase) in which the molecular axes are collinear and parallel to the substrate surface. The oxygen lattice in this δ phase has a centered rectangular [or isosceles triangular (IT)] structure which is incommensurate with the substrate graphite hexagon. This phase was predicted by Etters *et al.*²² by pattern search energy minimization. The zero-temperature energy minimization calculation²² which ignored the substrate corrugation predicted the IT lattice structure of this low-coverage δ phase. Experimentally, this phase was first found by Heiney *et al.*¹⁷ and later careful LEED work²¹ gave a great deal of information about this phase.

Finite-temperature properties of the δ phase have been studied by using Monte Carlo simulations.^{23,24} In particular, Pan *et al.*²³ have investigated the melting properties of finite-size clusters. Molecular-dynamics (MD) simulation is another direct method to study the structure and phase transitions and in addition it gives information about the real time dynamics.²⁵ In particular, the constant-pressure molecular dynamics is an excellent method for systems exhibiting structural change with temperature or pressure.²⁶ We have previously studied the properties of a diatomic molecular monolayer system²⁷ which closely resembles this δ phase of O_2 on graphite. We found a first-order phase transition from an orientationally ordered ferroelastic phase to an orientationally disordered paraelastic phase at temperature $T_c=20.1$ K. This order-disorder transition is accompanied by a lattice structure change where the oxygen lattice transforms from an IT structure to an equilateral triangular (ET) structure. This result is in reasonable agreement with a recent LEED experiment.²⁸ In addition, we have studied the dynamical properties in this system and the behavior of sound velocity across the ferroelastic phase transition for certain symmetry directions.²⁹

In the present paper we report in detail our constant-pressure molecular-dynamics studies of this 2D ferroelastic phase transition and the phonon dynamics. In addition to the oxygen monolayer problem, another goal of our study is to investigate, from a microscopic basis, the orientational order-disorder and associated ferroelastic structural phase transitions in a model 2D molecular solid.

This paper is organized as follows. In Sec. II, we introduce the model and the interaction potential and discuss the nature of the ground state. In Sec. III, we describe the constant-pressure molecular-dynamics method that we have used. In particular, we emphasize the importance of incorporating rotational contributions to the internal stress tensor. In Sec. IV, we give our MD results for the ferroelastic phase transition and also the solid-liquid melting transition. In Sec. V, we discuss the time-dependent density-density correlation function and associated dynamical structure factor. In addition, we present phonon dispersion curves for temperatures both below and above the ferroelastic transition. We also compare these MD results with those obtained by a quasiharmonic lattice dynamics (QHLD) calculation and address the question of phonon softening near the structural transition. In Sec. VI, we give a brief discussion and present our conclusions.

II. INTERACTION POTENTIAL AND THE GROUND STATE

The system we have studied is a homonuclear molecular monolayer. The molecules interact through an atom-atom potential of Lennard-Jones (LJ) type, i.e.,

$$V(r) = 4\epsilon \left[\left(\frac{\sigma}{r} \right)^{1/2} - \left(\frac{\sigma}{r} \right)^6 \right], \quad (1)$$

where r is the distance between two atoms. Since the internal vibrational frequency of each molecule is very

high due to strong bonding between the two atoms, we can assume the molecule to be rigid.³⁰ The potential parameters we have used are appropriate for the oxygen molecule,^{22,31} i.e.,

$$\epsilon = 54.34k_B, \quad \sigma = 3.05 \text{ \AA}, \quad (2)$$

with internuclear distance $d = 1.208 \text{ \AA}$. For monolayer density in the neighborhood of 10 molecules/(100 \AA^2), this system closely resembles the δ phase of oxygen molecular monolayer adsorbed on a graphite substrate. However, more accurate modeling of this δ phase requires the inclusion of other interactions which may be rather small. For example, the oxygen molecule has a nonzero spin ($S=1$) which leads to a magnetic exchange interaction between two molecules.³² This interaction is responsible for the low-temperature (below 11 K) antiferromagnetic structure in the ϵ phase of the O_2 on graphite system.³³ The corrugation of the substrate potential is nonzero but small (about 5 K).³⁴ Both these have been neglected in the present study. Also, we neglect the out-of-plane motions of molecules; thus all molecules are constrained to be parallel to the substrate.

To find the minimum energy configuration at zero temperature, we start from a state near the orientational ordered ferroelastic (FE) phase and search for the lowest energy as a function of the lattice parameters a, b and orientation of each molecule [see Fig. 1(a)]. At the minimum energy configuration, the internal stress tensor \mathcal{P} should vanish. The components of \mathcal{P} are calculated through the virial formula, i.e.,

$$\mathcal{P}_{\mu\nu} = \frac{1}{\Omega} \left[\sum_{i=1}^N m \dot{x}_i^\mu \dot{x}_i^\nu + \sum_i \sum_{j(>i)} F_{ij}^\mu x_{ij}^\nu \right], \quad (3)$$

where $m = 31.990$ a.u. is the mass of O_2 molecule, Ω is the area of the system, \mathbf{F}_{ij} is the force on molecule i by molecule j , \mathbf{x}_i is the center-of-mass (c.m.) of the i th molecule, $\mathbf{x}_{ij} = \mathbf{x}_i - \mathbf{x}_j$, $(\mu, \nu) = (x, y)$ and x_{ij}^μ is the μ component of \mathbf{x}_{ij} , etc. The first summation in Eq. (3) is the

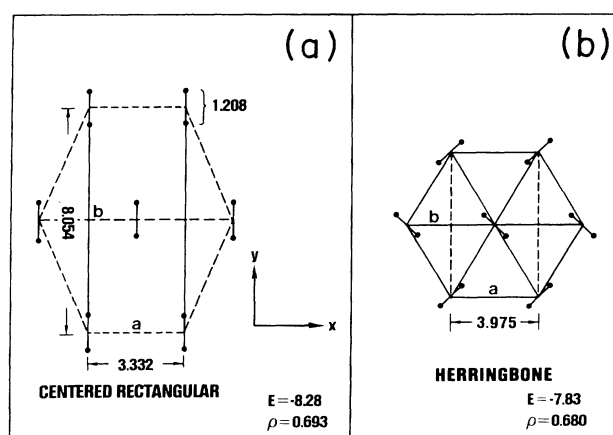


FIG. 1. The minimum energy configurations with the ferroelastic molecular ordering (left) or the herringbone ordering (right). The energy is in units of ϵ and the density is in units of $1/\sigma^2$.

velocity contribution and it vanishes at zero temperature. The surface tension (lateral pressure) p is given by

$$p = \frac{1}{2}(\mathcal{P}_{xx} + \mathcal{P}_{yy}). \quad (4)$$

Note that in Eq. (3) only the molecular center-of-mass coordinates contribute to the stress tensor. We have used both energy minimization and zero value of the internal stress tensor with only the c.m. contribution for locating the ground state. Although this is adequate for the ground state, for finite temperatures, we shall argue later that significant contribution to $\mathcal{P}_{\mu\nu}$ can arise from the orientational degrees of freedom.

The ground-state structure we find from the above criterion is an IT lattice with FE molecular ordering. The lattice constants are $a = 3.332 \text{ \AA}$ and $b = 8.054 \text{ \AA}$; molecules are all parallel to the b axis [see Fig. 1(a)]. For a 19×19 lattice with periodic boundary condition, the potential energy per molecule is -8.28ϵ with surface tension $p = 0.0064\epsilon/\sigma^2$. These lattice constants are slightly different from those given by Etters *et al.*²² ($a = 3.32 \text{ \AA}$, $b = 8.07 \text{ \AA}$) obtained by a pattern search method for the same model. The ground state has a surface coverage $\rho = 1.172\rho_0$; where ρ_0 is the coverage of the $\sqrt{3} \times \sqrt{3}$ structure on the graphite which corresponds to $0.0636 \text{ molecules/\AA}^2$. Experimentally,^{21,28} it is found that the ground state of the low-density δ phase of oxygen monolayer on the graphite has an IT lattice structure with $a = 3.25 \text{ \AA}$ and $b = 7.98 \text{ \AA}$. The oxygen molecules lie flat on the substrate surface and are orientationally ordered along the b axis. The oxygen molecule has a nonzero but small electric quadrupole moment.³¹ For computational convenience, the quadrupole moment can be constructed by putting a charge $2Ze$ at the molecular center and $-Ze$ at the two atomic positions. The value we have used is $Ze = 0.111 \text{ esu}$. It corresponds to a quadrupole moment $Q = -0.39 \times 10^{-26} \text{ esu cm}$. If we add the quadrupole-quadrupole (QQ) interactions, the change in the lattice constants of the FE state is less than 0.3%, and the change in energy is less than 2%.

Another 2D diatomic molecular solid is the well studied nitrogen (N_2) physisorbed on graphite.³⁵⁻³⁷ The ground state of this system has herringbone (HB) ordering with ET center-of-mass lattice structure which is commensurate with the graphite hexagon.³⁸ To see whether there is a stable structure with HB ordering for the oxygen monolayer, we have searched for the energy minimum by assuming a HB ordering and ET lattice structure. We have found that the potential energy is minimized with lattice constants $a = 3.975 \text{ \AA}$ and $b = \sqrt{3}a$ [see Fig. 1(b)]. The energy for this state is -7.83ϵ which is higher than the energy of the FE-IT structure (-8.28ϵ). Recently Joshi and Tildesley³⁹ used the same LJ potential parameters as ours to search for the minimum energy structure. They have found that, even in the absence of QQ interaction, the energy of the HB ordering can be lowered further (-8.167ϵ) by relaxing the constraints of ET center-of-mass structure. This energy is still higher than that of the FE-IT structure. Furthermore, inclusion of the QQ interaction to the molecular potential stabilized the former (HB-IT) structure (with minimum energy -8.274ϵ) compared to the

FE-IT structure. The relative stability of FE-IT and HB-IT structure is extremely sensitive to the oxygen quadrupole moment. However, the FE-IT configuration is the experimentally observed stable ground-state structure. Therefore, in the absence of a precise value of the quadrupole moment of an oxygen molecule on the graphite substrate, we have ignored the QQ interaction in our MD simulations.

III. THE CONSTANT-PRESSURE MOLECULAR DYNAMICS

In this section we give a brief description of the constant-pressure molecular-dynamics method which we have used to study the structural phase transitions involving molecular orientations.

A. Constant-pressure ensemble and stress tensor

A novel simulation method which has proved extremely powerful in studying phase transitions involving rearrangement of crystallographic structure is the constant-pressure molecular dynamics first proposed by Anderson⁴⁰ and later elaborated by Parrinello and Rahman.⁴¹⁻⁴⁴ For a 2D monoatomic system, the main features of this method can be briefly reviewed as follows. First, a two-dimensional MD cell characterized by vectors \mathbf{a} and \mathbf{b} is defined. All the particles are located inside this cell and the cell is repeated in space by periodic boundary conditions. The vectors \mathbf{a}, \mathbf{b} are allowed to change in the simulation. Positions of the atoms are expressed in the basis consisting of \mathbf{a} and \mathbf{b} . At a given instant, the position \mathbf{x} of each atom can be expressed as $\mathbf{x} = \mathbf{a}s^{(a)} + \mathbf{b}s^{(b)}$. The components of the scaled coordinate vector \mathbf{s} lie in the interval (0,1). We have

$$\mathbf{x} = \mathbf{h}\mathbf{s}, \quad (5a)$$

where \mathbf{h} is a 2×2 matrix given by

$$\mathbf{h} = \begin{pmatrix} a_x & b_x \\ a_y & b_y \end{pmatrix}. \quad (5b)$$

In Eq. (5b), $\mathbf{a} = a_x \hat{\mathbf{x}} + a_y \hat{\mathbf{y}}$, $\mathbf{b} = b_x \hat{\mathbf{x}} + b_y \hat{\mathbf{y}}$ and $\hat{\mathbf{x}}, \hat{\mathbf{y}}$ are two unit vectors of a Cartesian coordinate system. A mass W is assigned to the MD cell whose dynamics is determined by the external pressure and the internal stress tensor.

The Lagrangian describing the system is given by

$$\mathcal{L}_1 = \frac{1}{2} \sum_{i=1}^N m_i \dot{\mathbf{s}}_i^+ \mathbf{G} \dot{\mathbf{s}}_i - \Phi - p_e \Omega + \frac{1}{2} W \text{Tr} \dot{\mathbf{h}}^+ \dot{\mathbf{h}}, \quad (6)$$

where Φ is the interaction potential, $\mathbf{G} = \mathbf{h}^+ \mathbf{h}$ (\mathbf{h}^+ is transpose of matrix \mathbf{h}), $\mathbf{s}_i^+ = (s_i^{(a)}, s_i^{(b)})$, Ω is the area of the MD cell, i.e., $\Omega = \det(\mathbf{h})$, and p_e is the external spreading pressure.

Equation of motions (EOM's) generated from this Lagrangian are

$$m \ddot{\mathbf{s}}_i = \mathbf{h}^{-1} \sum_{j(\neq i)} \mathbf{F}_{ij} - m \mathbf{G}^{-1} \dot{\mathbf{G}} \dot{\mathbf{s}}_i. \quad (7)$$

The EOM's for the cell vectors \mathbf{a} and \mathbf{b} are given by

$$W \ddot{\mathbf{h}} = \Omega (\mathcal{P} - p_e \mathcal{J})(\mathbf{h}^+)^{-1}, \quad (8)$$

where \mathcal{P} is the internal stress tensor given by Eq. (3) and \mathcal{I} is the 2×2 identity matrix. Note that in Eq. (3), we can formally write $\mathbf{x}_i = \mathbf{h}\mathbf{s}_i$, and $\dot{\mathbf{x}}_i = \mathbf{h}\dot{\mathbf{s}}_i$ (neglecting much smaller $\dot{\mathbf{h}}\mathbf{s}_i$ terms). Equation (8) shows that change in the volume and the shape of the MD cell is driven by the imbalance between the external pressure and the internally generated stress.

The constant of motion is readily identified as the enthalpy H given by

$$H = \frac{1}{2} \sum_{i=1}^N \sum_{\mu} m \dot{x}_i^{\mu} \dot{x}_i^{\mu} + \Phi + p_e \Omega. \quad (9)$$

Note that a small contribution of $2k_B T$ to H coming from the four degrees of freedom of the MD cell vectors has been neglected. As proved by Anderson,⁴⁰ the time average of a physical quantity along the trajectory produced by the Lagrangian \mathcal{L}_1 is equal to the isoenthalpic-isobaric ensemble average of that quantity.

For polyatomic molecular system, Nosé *et al.*^{45–48} generalized the above method by adding a term $\frac{1}{2} \sum_i \omega_i^+ \mathbf{I} \omega_i$ to the Lagrangian \mathcal{L}_1 , i.e.,

$$\begin{aligned} \mathcal{L}_2 = & \frac{1}{2} \sum_{i=1}^N m \dot{\mathbf{s}}_i^+ \mathbf{G} \dot{\mathbf{s}}_i - \Phi - p_e \Omega \\ & + \frac{1}{2} W \text{Tr} \dot{\mathbf{h}}^+ \dot{\mathbf{h}} + \frac{1}{2} \sum_{i=1}^N \omega_i^+ \mathbf{I} \omega_i, \end{aligned} \quad (10)$$

where \mathbf{I} is the molecular moment of inertia tensor and ω_i is the angular velocity of the i th molecule. In the Lagrangian, the term $\sum_i \dot{\mathbf{s}}_i^+ \mathbf{G} \dot{\mathbf{s}}_i$ couples the molecular c.m. motion to the MD cell vectors. There is no such term which couples the rotational motion (ω_i) of the molecules to these vectors. Since only the center-of-mass coordinates are scaled by the MD cell vectors, only the c.m. coordinates appear explicitly in the stress tensor \mathcal{P} [see Eq. (3)].

For our diatomic molecular system, the orientational dynamics is expected to play a crucial role in the structural phase transition involving a shape change. To properly account for the effect of the rotational motion on the structural transition, we have developed a procedure to include the rotational contribution to the stress tensor.⁴⁹ To obtain the above-mentioned contribution to the stress tensor, one has to scale the coordinates of individual atoms \mathbf{x}_{ik} by the tensor \mathbf{h} [i.e., $\mathbf{x}_{ik} = \mathbf{h}\mathbf{s}_{ik}$, instead of Eq. 5(a)]. This will modify both the potential and kinetic-energy contributions to \mathcal{P} . For the former, one has to know the total force acting on individual atoms of every molecule. The total force acting on a particular atom of a given molecule \mathbf{F}_{ik} can be divided into two parts; one exerted by the atoms belonging to other molecules and the other a constraint force, which keeps the molecule rigid. The constraint force can be obtained from the rigid rotor conditions. In addition to modifying the potential-energy contribution, the above scaling also changes the kinetic-energy contribution. Besides the center-of-mass velocity-dependent terms, there are also ω_i ($=\dot{\theta}_i$, where θ_i is the angle that the i th molecule makes with the x axis, see Fig. 1) dependent terms. In fact, there is a partial cancellation between the potential

and kinetic-energy contributions depending on ω_i .

If we ignore all the ω_i contributions to the stress tensor, we have

$$\mathcal{P}_{xx} = \mathcal{P}_{xx}^{\text{c.m.}} - \frac{1}{2} d \sum_i \cos \theta_i \sin \theta_i (F_{i1}^{(\theta)} - F_{i2}^{(\theta)}), \quad (11a)$$

$$\mathcal{P}_{yy} = \mathcal{P}_{yy}^{\text{c.m.}} + \frac{1}{2} d \sum_i \cos \theta_i \sin \theta_i (F_{i1}^{(\theta)} - F_{i2}^{(\theta)}), \quad (11b)$$

$$\mathcal{P}_{xy} = \mathcal{P}_{xy}^{\text{c.m.}} - \frac{1}{2} d \sum_i \sin \theta_i \sin \theta_i (F_{i1}^{(\theta)} - F_{i2}^{(\theta)}), \quad (11c)$$

$$\mathcal{P}_{yx} = \mathcal{P}_{yx}^{\text{c.m.}} + \frac{1}{2} d \sum_i \cos \theta_i \cos \theta_i (F_{i1}^{(\theta)} - F_{i2}^{(\theta)}), \quad (11d)$$

where $\mathcal{P}^{\text{c.m.}}$ is defined in Eq. (3). Clearly, the symmetric component of \mathcal{P} , i.e., p [$=\frac{1}{2}(\mathcal{P}_{xx} + \mathcal{P}_{yy})$] depends only on $\mathcal{P}^{\text{c.m.}}$. On the other hand, the antisymmetric component of the stress tensor $\mathcal{A} = \frac{1}{2}(\mathcal{P}_{xy} - \mathcal{P}_{yx})$ has an important θ_i -dependent term which has to be kept to conserve the total angular momentum. This term was not included in earlier MD simulations of molecular systems^{46,50} and this may have led to difficulties in keeping the total angular momentum conserved. The ω_i -dependent terms which we have not written down here do not contribute to p and \mathcal{A} . In the present MD simulation we have not included these contributions to \mathcal{P} . These contributions may however be important for phase transitions under uniaxial external stress.⁴⁹

B. Conservations of energy, momentum, and angular momentum

We have used a fifth-order predictor-corrector algorithm⁵¹ to integrate the EOM's and have found that in 10^4 MD time steps, the deviation of energy is less than 0.3%. The simulation was performed with $N=400$ particles with periodic boundary conditions. The MD cell mass was chosen as $W = m\sqrt{N}$. When the stress tensor is calculated by Eqs. (11), the antisymmetric component of the stress tensor \mathcal{A} is zero for a system with zero initial total angular momentum. We found that typically in 10^4 MD time steps, standard deviation in \mathcal{A} is of the order 10^{-14} .

It is important to ensure that the total momentum \mathbf{p} of the system is zero since a nonzero \mathbf{p} will give every molecule an additional velocity and increase the pressure calculated by the virial formula, thereby making the system artificially soft. To make \mathbf{p} zero, we shift all the velocities \mathbf{v}_i , i.e.,

$$\mathbf{v}_i \rightarrow \mathbf{v}_i - \frac{1}{N} \sum_j \mathbf{v}_j, \quad (12)$$

the velocity \mathbf{v}_i is then multiplied by a factor

$$\frac{\sum_i v_{iy} x_i}{\sum_i v_{ix} y_i}$$

to make the total angular momentum zero. The adjusted velocities are then used to calculate the temperature T of the system by the formula

$$\frac{3}{2} N k_B T = \frac{1}{2} \sum_{i=1}^N m (v_{ix}^2 + v_{iy}^2 + \frac{1}{4} d^2 \dot{\theta}_i^2). \quad (13)$$

All the velocities are then multiplied by a factor $\sqrt{T_0/T}$

to force the system to have the required temperature T_0 .

In our simulations, we found that scaling all the derivatives of x_i , y_i , and θ_i by a factor of $\sqrt{T_0/T}$ helped the system approach equilibrium much faster. Usually (except for quick quench studies), we give 500–1000 steps for the purpose of raising the temperature. These steps are divided into 10–20 segments, the temperature difference is uniformly distributed among these segments so that the heating (cooling) process is smooth. In the equilibrium stage, fluctuation of temperature is small. We adjust the instantaneous temperature to the desired value T_0 and record the information needed for the calculations of the isobaric-isothermal ensemble averages. Usually, the average is calculated over 2000–3000 time steps. When close to the transition region, $1.0 - 1.5 \times 10^4$ time steps have been used.

C. Simulation of the Lennard-Jones system

For computational convenience,⁵² we use dimensionless units for length, time, temperature, etc. The length, energy, temperature, pressure, and mass are expressed in units of σ , ϵ , ϵ/k_B , ϵ/σ^2 , and m . These choices lead to a time unit $\sigma\sqrt{m/\epsilon}$, which is 1.8148×10^{-12} sec for this diatomic molecular system. The high accuracy of the algorithm that we have used and the large cutoff distance 5σ for the interaction potential enable us to use a relatively large time step, $\Delta t = 0.01102$, corresponding to 0.02 psec.

The Lennard-Jones potential $V(r)$ is cut off at $r_0 = 5\sigma$ and then modified to be of the form

$$\tilde{V}(r) = \begin{cases} V(r) - V(r_0) + f(r_0)r - f(r_0)r_0 & \text{if } r < r_0, \\ 0 & \text{otherwise,} \end{cases} \quad (14)$$

so that the potential and the force are both continuous at the cutoff. The function $f(r)$ is given by

$$f(r) = -\frac{\partial V(r)}{\partial r}. \quad (15)$$

Since $f(r_0) \approx -0.00031(\epsilon/\sigma)$, the term linear in r in Eq. (14) does not affect the calculation significantly. In fact, this effect is expected to be smaller than our statistical error, but the continuous nature of the potential and its derivative are helpful for the accuracy of numerical integration. The large cutoff also gives more information about the radial distribution function (RDF) of the c.m. molecules, because for computational convenience the RDF is calculated along with the potential and the force.

IV. THE FERROELASTIC PHASE TRANSITION

Under zero external pressure, starting from temperature $T^* = k_B T / \epsilon = 0.12$, the system was gradually heated with a temperature step 0.06 and two phase transitions were found. The first one is at $T^* = 0.37$ (20.1 K) where the system undergoes a ferroelastic transition, the orientational long-range order (OLRO) is lost and the lattice transforms to the ET structure. The second one is at $T^* = 0.70$ (38.0 K) where the paraelastic (plastic) phase

melts to an isotropic 2D liquid phase. Various physical quantities such as the internal energy, the density, the radial distribution function and order parameters were calculated. When the system is heated from $T^* = 0.36$ to 0.38, all these quantities change drastically in about 8000 MD time steps (corresponding to a real time of 160 psec). After that, the system has the ET structure and the orientational order disappears. The system is then allowed to run for 1.2×10^4 time steps over which thermal averages for the higher temperature paraelastic phase are computed.

A. Lattice anisotropy and orientational ordering

To measure the distortion of the lattice from a perfect ET structure ($\theta_i = 90^\circ$), we define a parameter γ by

$$\gamma = \frac{b}{(3)^{1/2}a} - 1. \quad (16)$$

In the ground state, $a = 3.332 \text{ \AA}$ and $b = 8.054 \text{ \AA}$, γ has a value 0.396. Just before the ferroelastic transition, $a = 3.462 \text{ \AA}$, $b = 8.055 \text{ \AA}$, and γ is as high as 0.343. The small reduction in γ as T increases indicates that the system is rather stiff. At $T^* = 0.38$, a increases to 4.006 \AA and b decreases to 7.066 \AA ; these values correspond to an ET lattice. An interesting observation is that the lattice spacing of 4.006 \AA is very close to that of the HB-ET structure as shown in Fig. 1(b).

For a measure of the orientational order we take

$$\eta_2 = \frac{1}{N} \sum_{i=1}^N \cos(2\theta_i - 2\bar{\theta}) \quad (17)$$

as the order parameter, where $\bar{\theta} = (1/N) \sum_i \theta_i$. Our simulation indicates that η_2 has a large decrease at $T^* \approx 0.38$. The orientational order parameter appears to change discontinuously at temperature 0.38 and does not show a slow decaying tail above this temperature. It is well known⁵³ that such a tail is always present after the transition as a finite size effect in computer simulations of second-order phase transitions. Our observations suggest that the transition is first order (see below). The true transition temperature is somewhere between 0.36 and 0.38. We estimate $T_c^* = 0.37$ which corresponds to 20.1 K. This value of T_c is about 6 K lower than the recent experimental value of 26 K.²⁸

B. Energy and density

The energy per molecule E and the monolayer density ρ are given in Fig. 2 as functions of temperature. Both E and ρ show discontinuities at $T^* = 0.37$. The change of the entropy can be calculated by using the formula $\Delta S = \Delta E / T_c$ and it is 0.88 (in units of k_B). Since for a free rotor the total entropy is $\ln(2\pi) = 1.838$, the above change in the entropy at the transition suggests that the rotors are undergoing hindered motion in the disordered phase. The latent heat associated with the transition coupled with the discontinuities in the energy, density, and the order parameter strongly suggests that the transition is first order.

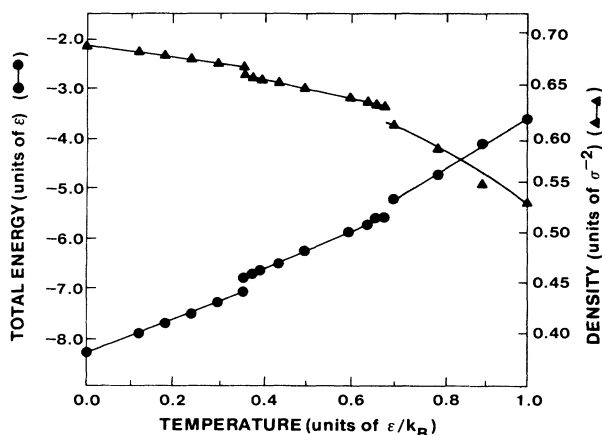


FIG. 2. Total energy and monolayer density. The lines are guide to the eye. Both energy and density are discontinuous at $T^*=0.37$ and $T^*=0.70$.

C. Radial distribution function

Because the ground-state structure is an IT lattice, the RDF of molecular center-of-mass can be viewed as if every peak in a set characterizing the ET lattice is split into a doublet structure. In particular, the peak arising from the six nearest neighbors in an ET lattice will split into two separate peaks, one coming from the two neighbors at a distance a , the other from the four neighbors with a distance $(a^2 + b^2/4)^{1/2}$. When we heat the system from $T^*=0.36$ to $T^*=0.38$, in the first 8000 time steps (160 psec), the splitting between the above two peaks becomes smaller as time increases. Finally this splitting disappears and the RDF shows a set of peaks appropriate for an ET lattice. The explicit form of the radial distribution function $g(r)$ is

$$g(r) = \frac{\langle n(r^2, r^2 + (\Delta r)^2) \rangle}{\pi(\Delta r)^2}, \quad (18)$$

where $\langle n(r^2, r^2 + (\Delta r)^2) \rangle$ is the average number of molecules in a ring with area $\pi(\Delta r)^2$ and at a distance r from a given molecule. $g(r)$ will approach the value of the density as r goes to infinity.

Figure 3 shows $g(r)$ for three temperatures, $T^*=0.36$, 0.38, and 0.70. At $T^*=0.36$ which is just below the ferroelastic transition point, $g(r)$ shows clearly two peaks; while at $T^*=0.38$ which is just above the transition, these two peaks merge into a single peak corresponding to the six nearest neighbors in the ET structure. Note that there is a gap [$g(r)=0$] between the first six neighbors and the other neighbors in the solid phases. However, at $T^*=0.70$, there is no such gap and the RDF shows a liquidlike structure. This indicates that the solid melts at $T^* \approx 0.70$.

D. Orientational diffusion coefficient

In the ferroelastic phase, due to the symmetry of the diatomic molecule, there are two degenerate orientational

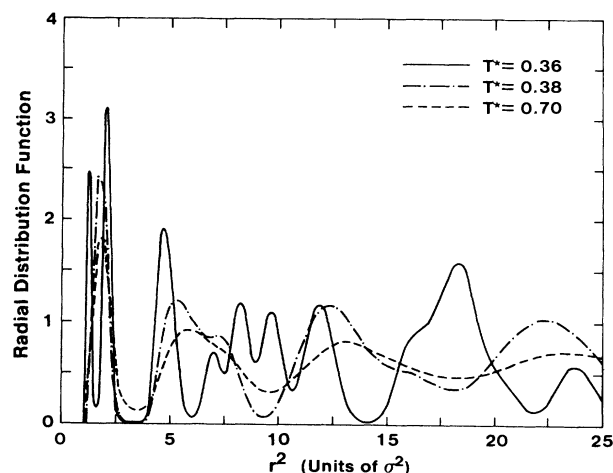


FIG. 3. Radial distribution function (as a function of r^2) of molecular center of mass for three different temperatures. All are averaged over 3000 MD time steps (60 psec).

states separated by an angle π for every molecule. As the temperature increases, so does the probability for the molecules to overcome the energy barrier and shuttle between these two states. Before the rotors become free, one expects them to behave like hindered rotors and have small orientational self-diffusion coefficient D_θ . On the other hand, if the rotors are nearly free, then even in a relatively short time scale, the system will have a considerably large D_θ .

The orientational self-diffusion coefficient D_θ can be calculated from the relation

$$D_\theta = \lim_{t \rightarrow \infty} \left[\frac{1}{t} f(t) \right], \quad (19a)$$

where

$$f(t) = \langle [\theta(t) - \theta(0)]^2 \rangle \quad (19b)$$

is the orientational autocorrelation function. In the MD simulation, the average of orientational autocorrelation function is computed as

$$f(t) = \sum_{k=0}^{M_k-1} \left[\frac{1}{M_k} \sum_{i=1}^N \left[\frac{1}{N} [\theta_i(t+k\tau) - \theta_i(k\tau)]^2 \right] \right], \quad (20)$$

where τ is a constant determined by the correlation time of the dynamics of the molecules and M_k is the number of MD configurations. D_θ can be obtained from $f(t)$ using a linear regression method.⁵⁴

Figure 4 shows $f(t)$ for temperatures $T^*=0.36$ and $T^*=0.38$. We see that the high-temperature autocorrelation function is 2 orders of magnitude larger than the low-temperature one. When T^* is 0.30, in a time interval as large as 3200 time steps (64 psec) there is no evidence of orientational diffusion. After heating it to $T^*=0.36$, we found $D_\theta = 4.9 \pm 0.4 \times 10^9$ rad²/sec for $t > 2000$ time

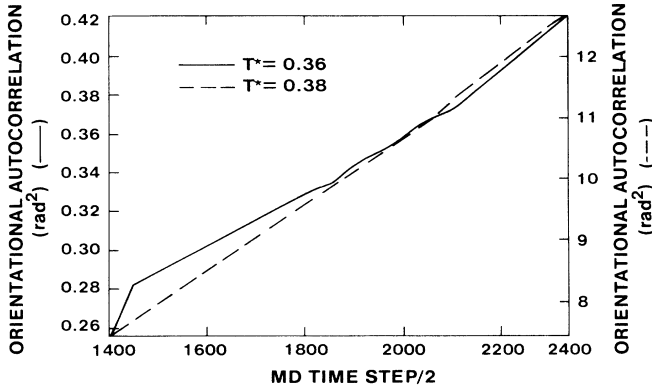


FIG. 4. Orientational autocorrelation functions at temperatures below and above the ferroelastic phase transition temperature. MD time steps are from 2800 to 4600.

steps. At $T^*=0.38$, D_θ is $1.49 \pm 0.08 \times 10^{11}$ rad²/sec. The increase in D_θ by a factor of 30 strongly suggests that the ferroelastic phase transition is first order. Figure 5 gives $\log D_\theta$ versus the inverse temperature. The increase in D_θ at the solid-liquid transition temperature $T^* \approx 0.70$ is only about 1.5 suggesting that there may be considerable rotational diffusion in the paraelastic phase below the solid-liquid melting temperature. The increase

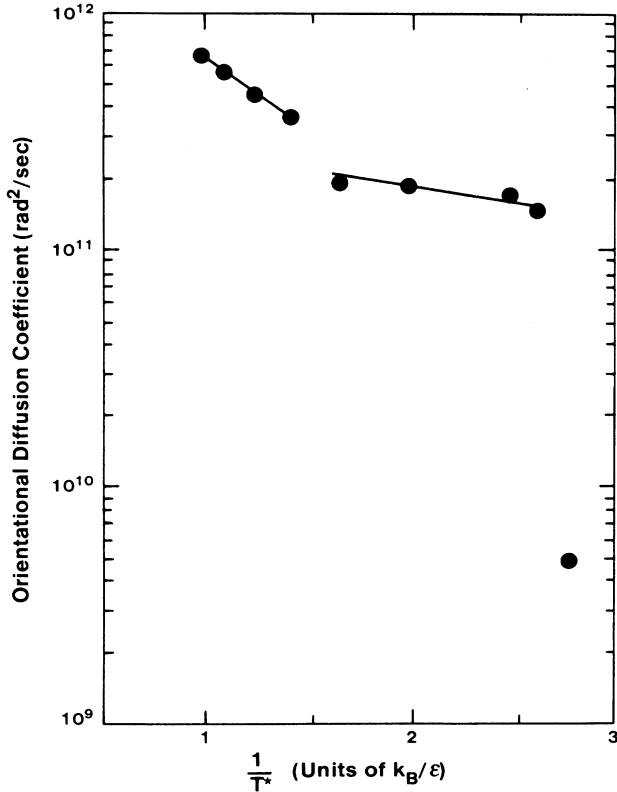


FIG. 5. Orientational diffusion coefficient. The horizontal axis represents the inverse of temperature. The lines are guide to the eye.

in the slope of $\log D_\theta$ versus $1/T^*$ by a factor of 3 in going from the paraelastic phase to the liquid phase is an interesting observation and needs more further careful investigation.

E. Strain fluctuation and elastic constant

The gauge matrix \mathbf{G} appearing in Eq. (10) reflects the change in the volume and the shape of the MD cell and contains information about the strain in the system. The relation between \mathbf{G} and the strain tensor ϵ can be expressed as^{42,55}

$$\epsilon(t) = \frac{1}{2}[(\mathbf{h}_0^+)^{-1} \mathbf{G} \mathbf{h}_0^{-1} - \mathcal{J}], \quad (21)$$

where \mathbf{h}_0 characterizes the MD cell of the reference state in which the strain is zero. In MD simulation \mathbf{h}_0 is generally replaced by the average of $\mathbf{h}(t)$. The compliances Γ_{ijkl} are related to the strain fluctuations by the relation,^{55,56}

$$\Gamma_{ijkl} = \frac{\Omega_0}{k_B T} \langle \Delta \epsilon_{ij} \Delta \epsilon_{kl} \rangle, \quad (22)$$

and the elastic constants C_{ijkl} can be obtained from the inverse of Γ_{ijkl} . The 4×4 matrix Γ_{ijkl} is singular due to the permutation symmetry for the Cartesian index. Using the Voigt convention⁵⁷

$$\Gamma_{\rho\sigma} = \begin{cases} \Gamma_{ijkl} & \text{if } k=1 \ (\sigma \leq 2), \\ 2\Gamma_{ijkl} & \text{if } k \neq l \ (\sigma > 2), \end{cases} \quad (23)$$

one can get a 3×3 regular matrix and its inverse can be calculated. To obtain symmetric C_{ijkl} , one then inverts the transformation of Eq. (23).

To get accurate values of C_{ijkl} using the above procedure is rather difficult⁵⁸ due to the large fluctuations of strains near the transition and due to the small size of the system in the simulation. However, the qualitative features of the elastic constants can be seen by comparing the values at $T^*=0.36$ and at $T^*=0.38$ calculated by the above method and given in Table I. Clearly, before the ferroelastic transition the system is highly anisotropic but after the transition it is isotropic, i.e., $C_{11} \approx C_{22}$, and the ratios C_{44}/C_{11} and $(C_{11} - C_{12})/C_{11}$ drop sharply near the transition.

F. Quench study

In Fig. 6 we give the RDF and a configuration of the system quenched from $T^*=0.38$ to $T^*=0.01$ in 500 MD time steps. We see there are only tiny domains with three equivalent distortion directions. Also we find hexagons with local herringbone structure. The radial distribution

TABLE I. Elastic constants (in units of ϵ/σ^2) calculated from the molecular dynamics at temperatures $T^*=0.36$ and $T^*=0.38$.

T^*	C_{11}	C_{22}	C_{12}	C_{44}
0.36	1.45	0.97	2.10	1.33
0.38	1.05	1.07	1.02	0.11

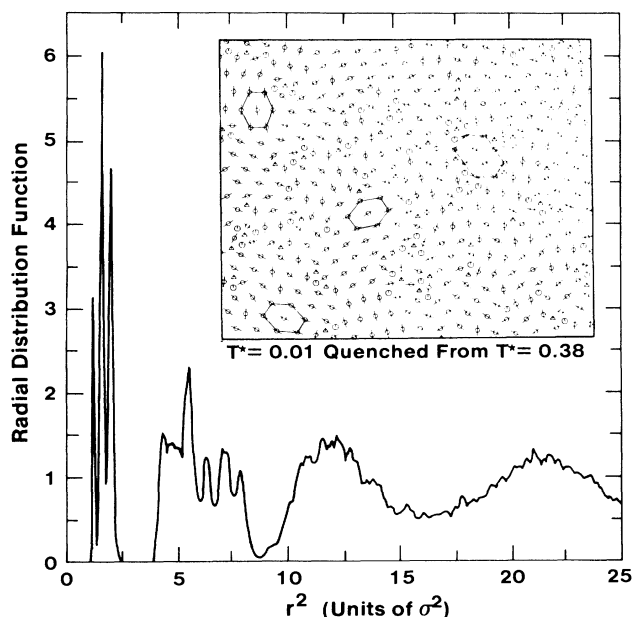


FIG. 6. Radial distribution function for a state quenched to $T^*=0.01$ from the paraelastic phase at $T^*=0.38$ in 10 psec. The inset gives the quenched configuration.

function shows a three-sharp-peak structure for small r . These three peaks are narrow due to the absence of phonons at this low temperature. Among the first three peaks, the middle one reflects the local ET structure while the other two reflect the local IT structure. This can be seen from the insert configuration plot where both local HB and FE orderings can be seen.

V. TRANSLATIONAL DYNAMICS AND PHONONS

In the previous sections we discussed MD results of mostly the thermodynamic properties. In this section we explore the effects of ferroelastic phase transition on the dynamical properties of the system. A brief version of our results has been given before,²⁹ where we have addressed the questions of phonon dispersion in one symmetry direction in the ferroelastic phase, elastic softening near the phase transition, and the low temperature heat capacity. Here we present additional results.

The dynamics of a molecular crystal in the orientationally disordered phase is a rather difficult problem. Furthermore, experimentally, only limited data are available. Neutron scattering which is widely used to study phonon dynamics and dispersions in 3D molecular crystals⁵⁹ has not been carried out extensively for 2D systems. From the theoretical side, one can study the phonon dynamics using the QHLD.⁶⁰ However, this method is only appropriate for the low temperature orientationally ordered phase where the phonons and librations are well defined and weakly coupled excitations. MD simulation is a direct probe of the dynamical properties and in particular, it is quite useful in understanding the dynamics in the orientationally disordered phase as the effects of strong translation-rotation coupling and anharmonicity are au-

tomatically included in these calculations.^{50,61}

We have used both QHLD and MD simulation to explore the dynamics of the molecular monolayer at different temperatures. In the QHLD, the phonon and libron frequencies are related to the eigenvalues of the dynamical matrix. We consider small displacements of molecular c.m.'s and small angle deviations of molecular orientations from their FE ordered state. The coupling between the c.m. translational motion and the librational motion is included in the leading order.⁶² This method therefore is good only at low temperatures when the molecules undergo small amplitude librations. As will be shown later, the QHLD works reasonably well up to the ferroelastic transition temperature if proper allowance of the lattice expansion is made. But in the high temperature orientationally disordered phase where molecules undergo orientational diffusion and large amplitude displacements, the weak coupling assumption is not adequate and a proper treatment is more complicated.^{12,63} Molecular dynamics is perhaps the only viable method available at the present time to understand strongly coupled translational-rotational dynamics.⁶⁴

Dynamical properties can be studied by the time-dependent correlation functions.⁶⁵ We have calculated the density-density correlation function defined by

$$F(\mathbf{q}, t) = \langle \rho_{\mathbf{q}}(t) \rho_{-\mathbf{q}}(0) \rangle, \quad (24)$$

where

$$\rho_{\mathbf{q}}(t) = \frac{1}{(N)^{1/2}} \sum_{i=1}^N e^{-i\mathbf{q} \cdot \mathbf{x}_i(t)} \quad (25)$$

is the space Fourier transform of the density; \mathbf{q} is wave vector, $\mathbf{x}_i(t)$ is the c.m. position of i th molecule at time t . The $\langle \rangle$ in Eq. (24) refers to an ensemble average (which equals to the time average in MD). In scattering experiments, $F(\mathbf{q}, t)$ is not measured directly, but its time Fourier transform, $S(\mathbf{q}, \omega)$ is related to the neutron scattering cross section,⁶⁶

$$S(\mathbf{q}, \omega) = \int_{-\infty}^{\infty} e^{i\omega t} F(\mathbf{q}, t) dt. \quad (26)$$

Since $F(\mathbf{q}, t)$ is an even function of time, $S(\mathbf{q}, \omega)$ is a real quantity. Longitudinal phonons show up directly in the function $F(\mathbf{q}, t)$. To obtain transverse phonons from $F(\mathbf{q}, t)$, a reciprocal lattice vector \mathbf{K} which is perpendicular to \mathbf{q} should be added to \mathbf{q} . Other types of collective excitations such as librations will affect the correlation function $F(\mathbf{q}, t)$ through their coupling with the phonons.

Using the trajectories of molecules generated by the MD simulation, we computed $F(\mathbf{q}, t)$ by

$$F(\mathbf{q}, t) = \sum_{k=0}^{M_k-1} \frac{1}{M_k} \rho_{\mathbf{q}}(t+k\tau) \rho_{-\mathbf{q}}(k\tau), \quad (27)$$

where M_k is the total number of configurations of the system used in the calculation; τ is the time between two successive recorded configurations, $\tau = n\Delta t$ with $\Delta t = 0.02$ (psec) is the (real) time between each integration step and $n = 5$. The total MD steps used is nM_k (corresponding to $T = nM_k\Delta t$ in real time). To avoid rapid oscillations in $S(\mathbf{q}, \omega)$ due to finite T , we average

$S(\mathbf{q}, \omega)$ with a Gaussian weight function.⁶⁷ This is equivalent to multiplying a Gaussian smoothing function to $F(\mathbf{q}, t)$ while carrying out the Fourier transform, i.e.,

$$S(\mathbf{q}, \omega) = \lim_{T \rightarrow \infty} \left[\int_{-T}^T e^{i\omega t} F(\mathbf{q}, t) e^{-\alpha(t/T)^2} dt \right]. \quad (28)$$

Thus the frequency resolution $\Delta\omega$ becomes

$$\Delta\omega = \frac{2\sqrt{\alpha}}{T}. \quad (29)$$

We usually choose α between 2 and 6.

The unit vectors of a general two-dimensional IT lattice are [Fig. 7(a)]

$$\begin{aligned} \mathbf{a}_1 &= a \hat{\mathbf{x}}, \\ \mathbf{a}_2 &= \frac{a}{2} (\hat{\mathbf{x}} + \tan\phi \hat{\mathbf{y}}), \end{aligned} \quad (30)$$

and the corresponding reciprocal lattice vectors are

$$\begin{aligned} \mathbf{b}_1 &= b^* (\frac{1}{2} \tan\phi \hat{\mathbf{x}} - \frac{1}{2} \hat{\mathbf{y}}), \\ \mathbf{b}_2 &= b^* \hat{\mathbf{y}}, \end{aligned} \quad (31)$$

where

$$b^* = \frac{4\pi}{a \tan\phi}. \quad (32)$$

The first Brillouin zone (BZ) is shown in Fig. 7(b) along with high symmetry points.

The MD results for the time-dependent correlation functions at temperature $T^* = 0.12$ and wave vectors along the $\Gamma-N$ direction are given in Fig. 8. This temperature is far below the ferroelastic phase transition temperature ($T_c^* = 0.37$). These $F(\mathbf{q}, t)$'s show well-defined oscillations with periodicities corresponding to those of longitudinal acoustic (LA) phonons traveling in the $\Gamma-N$ direction. The dynamical structural factor obtained from any one of these correlation functions shows a single peak at finite frequency corresponding to the LA-phonon frequency. Figure 9 gives one example of such $S(\mathbf{q}, \omega)$ for \mathbf{q} in the $\Gamma-N$ direction and magnitude equal to $0.3|\Gamma N|$. The phonon width is primarily determined by the resolution function in Eq. (28). In Fig. 10

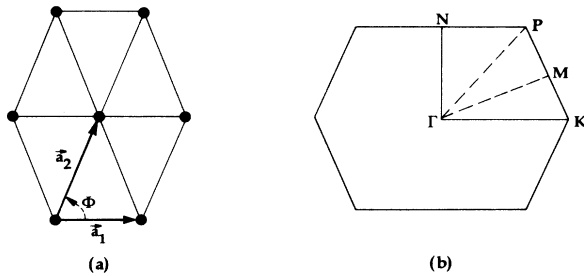


FIG. 7. (a) Two-dimensional (isosceles) triangular lattice with lattice vectors \mathbf{a}_1 and \mathbf{a}_2 , ($a = |\mathbf{a}_1|$). (b) The first Brillouin zone corresponding to (a) and the symmetry points.

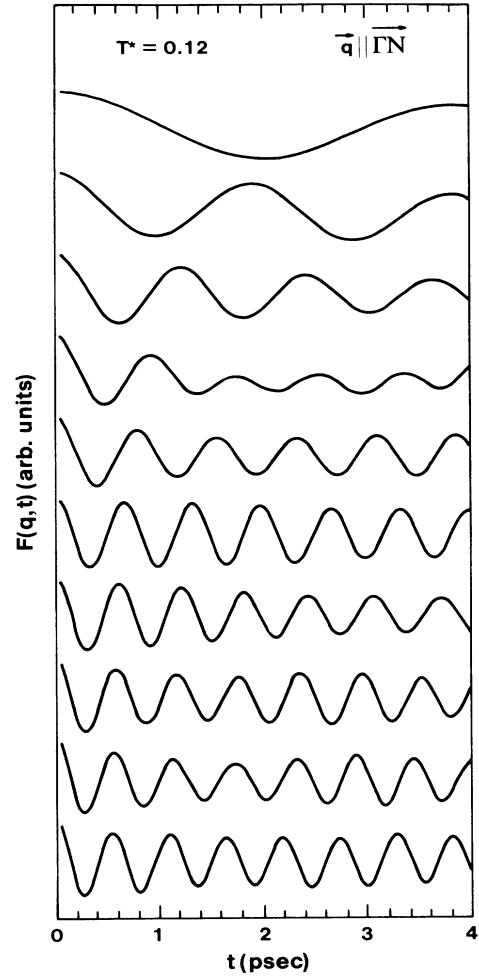


FIG. 8. Time-dependent density-density correlation function of molecular center of mass for $T^* = 0.12$. The wave vector \mathbf{q} increases from the zone center (point Γ) to the zone boundary (point N). Curves from top to bottom are for $|\mathbf{q}| = 0.1, 0.2, 0.3, 0.4, 0.5, 0.6, 0.7, 0.8, 0.9,$ and 1.0 (in units of $|\Gamma N|$).

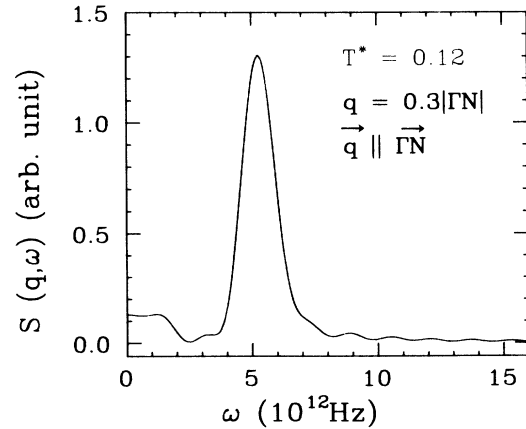


FIG. 9. Dynamic structure factor for $T^* = 0.12$ and for $|\mathbf{q}| = 0.3|\Gamma N|$.

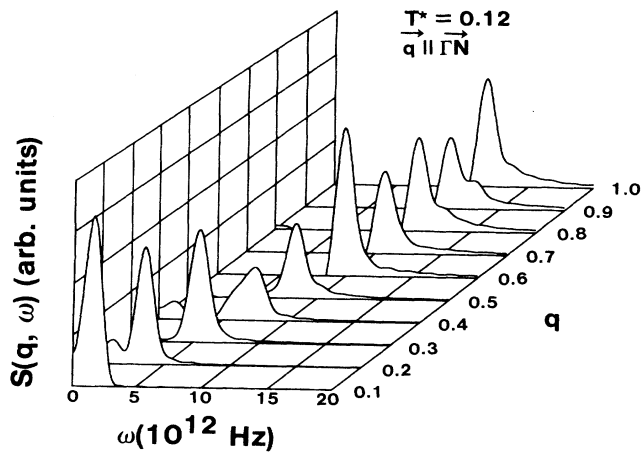


FIG. 10. The dynamic structure factors at $T^*=0.12$ and for \mathbf{q} parallel to $\Gamma-N$ in the first BZ. The wave vectors are expressed in units of $|\overline{\Gamma N}|$.

we give the dynamic structure factors for \mathbf{q} parallel to the $\Gamma-N$ direction [see Fig. 7b)] obtained from the $F(\mathbf{q}, t)$ shown in Fig. 8. One can clearly see the LA phonon dispersion. Figure 11 gives the LA phonon dispersion curves for $T^*=0.12$ and \mathbf{q} going from the N point to the zone center (Γ) and to the K point. The solid lines in this figure are obtained from the QHLD calculations.⁶² We see that the overall agreement between MD results and the QHLD results are quite good at this low temperature.

The behavior of phonons across the ferroelastic phase transition is a very interesting problem. For example, in molecular solid KCN, ultrasonic measurements⁶⁸ have shown that the shear elastic constant (C_{44}) softens drastically when the temperature approaches the ferroelastic phase transition temperature. This leads to a soft transverse acoustic (TA) phonon dispersion which has been seen in neutron scattering measurement.⁶⁹ MD simulation in KCN has also observed this elastic softening.⁷⁰ In our MD simulation we found that for the 2D system, the

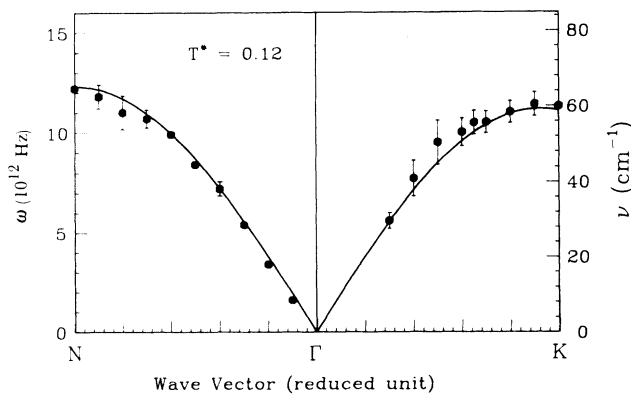


FIG. 11. LA phonon dispersion curves at $T^*=0.12$. The wave vectors are expressed in reduced unit ($|\overline{\Gamma N}|=1.0$). Solid lines are LA phonon dispersion curves obtained from quasiharmonic lattice dynamics. Solid dots are the results of molecular dynamics.

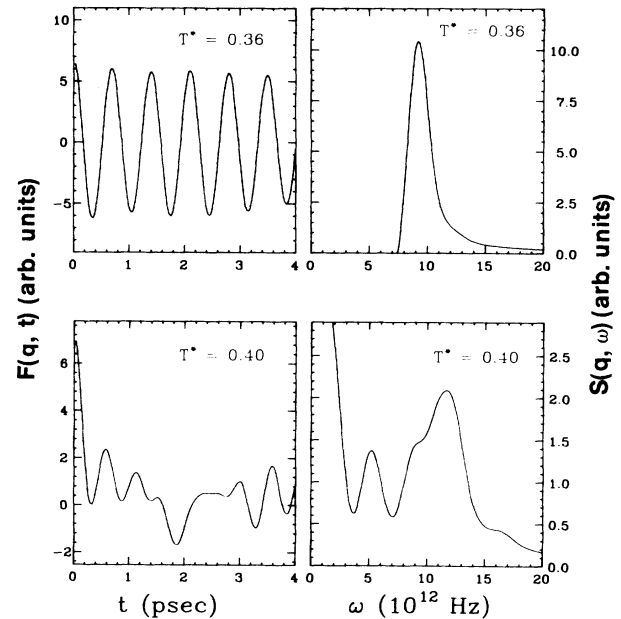


FIG. 12. Density-density correlation functions and the dynamic structure factors at temperatures $T^*=0.36, 0.40$ and for \mathbf{q} corresponding to the point N of the Brillouin zone.

LA phonons also soften as one approaches the phase transition temperature.²⁹ This result will be discussed in detail below.

Figure 12 shows the time correlation functions and the corresponding structure factors at temperatures $T^*=0.36$ which is just below the transition, $T^*=0.40$ which is above the transition, and for a wave vector corresponding to the point N of the first BZ. At $T^*=0.36$, $F(\mathbf{q}, t)$ is a well-defined weakly damped oscillating function of time and $S(\mathbf{q}, \omega)$ has a single peak. But at $T^*=0.40$, $F(\mathbf{q}, t)$ shows oscillations with rapid decay. The structure factor at $T^*=0.40$ is considerably more complicated. There is a large central peak coming from

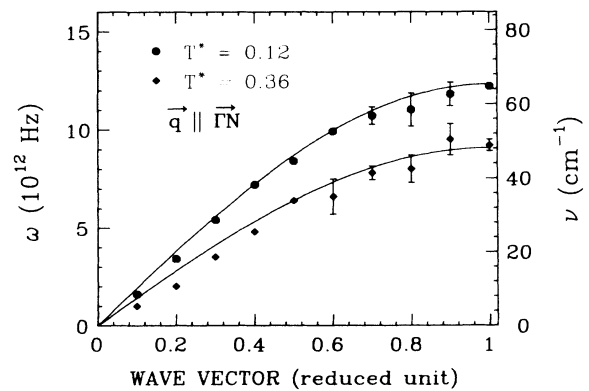


FIG. 13. LA phonon dispersions in the ferroelastic phase for two different temperatures and for \mathbf{q} from the zone center (point Γ) to the boundary point (N). Dots are the molecular dynamics results and the solid lines are the quasiharmonic lattice dynamics results.

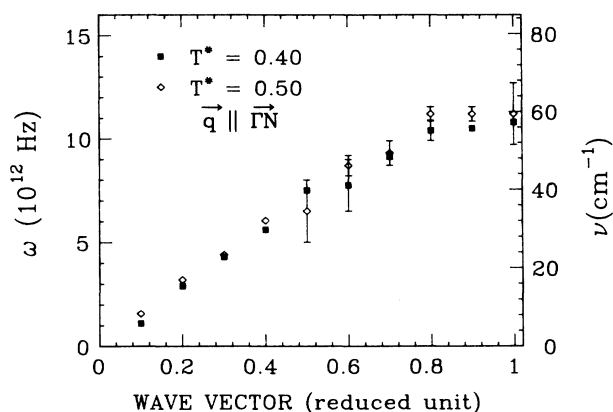


FIG. 14. LA phonon dispersion in the orientationally disordered paraelastic phase obtained from molecular dynamics.

the decaying behavior of the time correlation function and a broad peak which can be identified as a renormalized LA phonon peak. In addition, there is a low frequency peak whose origin is not clear at present. For \mathbf{q} vectors along the $\Gamma-N$ direction, similar behavior has also been observed. But the central peak is not present there.²⁹ These observations suggest that phonons are heavily damped in the high-temperature orientationally disordered phase. This is due to the increased importance of the intrinsic anharmonic effects⁷¹ and the strong coupling between the translational and rotational degrees of freedom.^{63,72}

Figure 13 shows the LA phonon dispersion at $T^*=0.12$ and 0.36 for the wave vector \mathbf{q} along the $\Gamma-N$ direction in the first BZ. It clearly shows an overall phonon softening along with additional softening of the long wavelength ($q \leq 0.4|\Gamma N|$) phonons as $T \rightarrow T_c$. QHLD calculations can account for the overall softening but fail to explain the anomalous softening in the low wave vector region. In Fig. 14, we give the MD results for the LA phonons in the $\Gamma-N$ direction at high temperatures ($T^*=0.40, 0.50$). There is a small hardening of the phonons with increasing temperature which can be traced to the effect of rotation-translation coupling.⁶³

VI. DISCUSSION AND SUMMARY

We have carried out a detailed study of the thermodynamics and dynamics of a two-dimensional molecular monolayer system undergoing a ferroelastic structural phase transition. Although the intermolecular interaction parameters are those appropriate for oxygen molecules, there are important differences between the system we have studied and oxygen molecules adsorbed on

graphite. Two significant physical effects not considered in the present simulation study are (1) orientations of the molecules away from the graphite plane with a concomitant motion of the center of mass perpendicular to the graphite substrate, and (2) corrugation of the graphite substrate. For a detailed comparison between the MD results and experiments on O_2 /graphite, the above two effects must be taken into account.

Our MD simulations can however be used to explore the physics of ferroelastic phase transition in two-dimensional molecular solids. The presence of an intermediate plastic phase is clear and the physical properties of this phase is dominated by strong rotational-translational coupling. In contrast to 3D systems, where one of the many transverse elastic constants softens as a result of the above mentioned coupling, there is only one transverse elastic constant ($C_{44} = C_{11} - C_{12}$) for a 2D triangular lattice and this softens (see Table I) as one approaches the ferroelastic transition temperature from above. The system therefore behaves almost like a liquid although the center-of-mass diffusion is absent. In fact, this is perhaps the reason why in experiments it is not easy to distinguish this intermediate plastic phase from the usual liquid phase. In addition, we find that the longitudinal acoustic phonons also soften as one approaches the ferroelastic phase transition temperature.

The phonons in the plastic phase are strongly damped whereas in the low-temperature ferroelastic phase they are rather well defined and can be understood within a QHLD theory. A direct experimental observation of the soft phonons and their behavior as a function of temperature will be of great help in elucidating the physics of strongly coupled rotation-translation system in 2D. The other significant aspect of our study is the possible effect of hydrostatic or uniaxial stress on the ferroelastic phase transition. As we have discussed in the text, there are important orientational coordinate and velocity dependent contributions to the internal stress tensor \mathcal{P} (only the ω_i independent part of these contributions were included in the present study) whose effect on the thermodynamic and dynamic properties will be of interest to explore.

ACKNOWLEDGMENTS

One of us (S.D.M.) acknowledges support from the National Science Foundation under Grant No. DMR-81-17247, another (R.K.K.) acknowledges support from the U. S. Department of Energy (Division of Materials Science, Office of Basic Energy Sciences), under Contract No. W-31-109-ENG-38. This work was supported in part by the Center for Fundamental Materials Research at Michigan State University.

¹F. Schwabl, *Ferroelastic* **24**, 171 (1980).

²T. A. Scott, *Phys. Rep.* **27C**, 89 (1976).

³G. C. DeFotis, *Phys. Rev. B* **23**, 4714 (1981).

⁴K. H. Michel and J. Naudts, *Phys. Rev. Lett.* **39**, 212 (1977); E.

Ohno and K. Yoshimitsu, *Prog. Theor. Phys. (Suppl.)* **80**, 180 (1984).

⁵S. D. Mahanti and G. Kemeny, *Phys. Rev. B* **20**, 2105 (1979).

⁶M. L. Klein, I. R. McDonald, and Y. Ozaki, *Phys. Rev. Lett.*

- 48, 1197 (1982).
- ⁷S. D. Mahanti, in *Condensed Matter Theory*, edited by P. Vashishta, R. K. Kalia, and R. F. Bishop (Plenum, New York, 1987), Vol. 2.
- ⁸V. K. Wadhawan, *Phase Transitions* **3**, 3 (1982).
- ⁹W. Dultz, H. H. Otto, H. Krause, and J. L. Buevoz, *Phys. Rev. B* **24**, 1287 (1981).
- ¹⁰O. E. Vilches, *Annu. Rev. Phys. Chem.* **31**, 463 (1980).
- ¹¹S. D. Mahanti and S. Tang, *Superlattices Microstructures* **1**, 517 (1985).
- ¹²D. Sahu, Ph.D. dissertation, Michigan State University, 1983.
- ¹³*Ordering in Strongly Fluctuating Condensed Matter Systems*, edited by T. Riste (Plenum, New York, 1979).
- ¹⁴R. Marx and B. Christoffer, *Phys. Rev. Lett.* **51**, 790 (1983).
- ¹⁵O. G. Mouritsen and A. J. Berlinsky, *Phys. Rev. Lett.* **48**, 181 (1982).
- ¹⁶J. Krim, J. P. Coulomb, and J. Bouzidi, *Phys. Rev. Lett.* **58**, 583 (1987).
- ¹⁷P. A. Heiney, P. W. Stephens, S. G. J. Mochrie, J. Akimitsu, R. J. Birgeneau, and P. M. Horn, *Surf. Sci.* **125**, 539 (1983).
- ¹⁸D. D. Awschalom, G. N. Lewis, and S. Gregory, *Phys. Rev. Lett.* **51**, 586 (1983).
- ¹⁹J. Stoltenberg and O. Vilches, *Phys. Rev. B* **22**, 2920 (1980).
- ²⁰M. Nielsen and J. P. McTague, *Phys. Rev. B* **19**, 3096 (1979).
- ²¹M. F. Toney, R. D. Diehl, and S. C. Fain, *Phys. Rev. B* **27**, 6413 (1983).
- ²²R. D. Eppers, R. P. Pan, and V. Chandrasekharan, *Phys. Rev. Lett.* **45**, 645 (1980).
- ²³R. P. Pan, R. D. Eppers, K. Kobashi, and V. Chandrasekharan, *J. Chem. Phys.* **77**, 1035 (1982).
- ²⁴O. M. B. Duparc and R. D. Eppers, *J. Chem. Phys.* **86**, 1020 (1987).
- ²⁵T. Schneider and E. Stoll, *Phys. Rev. B* **13**, 1216 (1976); **17**, 1302 (1978).
- ²⁶M. Parrinello, in *Molecular-Dynamics Simulation of Statistical-Mechanical Systems*, edited by G. Ciccotti and W. G. Hoover (North-Holland, Amsterdam, 1986), p. 204.
- ²⁷S. Tang, S. D. Mahanti, and R. K. Kalia, *Phys. Rev. Lett.* **56**, 484 (1986).
- ²⁸M. F. Toney and S. C. Fain, *Phys. Rev. B* **36**, 1248 (1987).
- ²⁹W. Jin, S. D. Mahanti, and Sanyee Tang, *Solid State Commun.* **66**, 877 (1988).
- ³⁰G. Herzberg, *Molecular Spectra and Molecular Structure, I. Spectra of Diatomic Molecules*, 2nd ed. (D. Van Nostrand, Princeton, 1965).
- ³¹C. A. English and J. A. Venables, *Proc. R. Soc. London A* **340**, 57 (1974).
- ³²C. A. English, J. A. Venables, and D. R. Salahub, *Proc. R. Soc. London A* **340**, 81 (1974).
- ³³Y. B. Gaididei and V. M. Loktev, *Phys. Lett. A* **123**, 85 (1987).
- ³⁴W. A. Steele, *Surf. Sci.* **36**, 317 (1973).
- ³⁵J. K. Kjems, L. Passell, H. Taub, and J. G. Dash, *Phys. Rev. Lett.* **32**, 724 (1974).
- ³⁶J. Eckert, W. D. Ellenson, J. B. Hastings, and L. Passell, *Phys. Rev. Lett.* **43**, 1329 (1979).
- ³⁷A. D. Migone, H. K. Kim, M. H. W. Chan, J. Talbot, D. J. Tildesley, and W. A. Steele, *Phys. Rev. Lett.* **51**, 192 (1983).
- ³⁸R. D. Diehl, M. F. Toney, and S. C. Fain, *Phys. Rev. Lett.* **48**, 177 (1982).
- ³⁹Y. P. Joshi and D. J. Tildesley, *Surf. Sci.* **166**, 169 (1986).
- ⁴⁰H. C. Anderson, *J. Chem. Phys.* **72**, 2384 (1980).
- ⁴¹M. Parrinello and A. Rahman, *Phys. Rev. Lett.* **45**, 1196 (1980).
- ⁴²M. Parrinello and A. Rahman, *J. Appl. Phys.* **52**, 7182 (1981).
- ⁴³M. Parrinello and A. Rahman, in *Melting, Localization and Chaos*, edited by R. K. Kalia and P. Vashishta (Elsevier, New York, 1982), p. 97.
- ⁴⁴M. Parrinello, A. Rahman, and P. Vashishta, *Phys. Rev. Lett.* **50**, 1073 (1983).
- ⁴⁵S. Nosé and M. L. Klein, *J. Chem. Phys.* **78**, 6928 (1983).
- ⁴⁶S. Nosé and M. L. Klein, *Mol. Phys.* **50**, 1055 (1983); *Phys. Rev. Lett.* **50**, 1207 (1983).
- ⁴⁷S. Nosé, *J. Chem. Phys.* **81**, 511 (1984).
- ⁴⁸S. Nosé and F. Yonezawa, *J. Chem. Phys.* **84**, 1803 (1986).
- ⁴⁹Sanyee Tang, Ph.D. dissertation, Michigan State University, 1985; W. Jin, S. Y. Tang, and S. D. Mahanti (unpublished).
- ⁵⁰M. L. Klein, *Annu. Rev. Phys. Chem.* **36**, 525 (1985).
- ⁵¹C. W. Gear, *Numerical Initial Value Problems in Ordinary Differential Equations* (Prentice Hall, Englewood Cliffs, 1971).
- ⁵²F. James, *Rep. Prog. Phys.* **43**, 73 (1980).
- ⁵³O. G. Mouritsen, *Computer Studies of Phase Transition and Critical Phenomena* (Springer, Berlin, 1984).
- ⁵⁴W. H. Press, B. P. Flannery, S. A. Teukolsky, and W. T. Vetterling, *Numerical Recipes* (Cambridge University Press, Cambridge, England, 1986).
- ⁵⁵M. Parrinello and A. Rahman, *J. Chem. Phys.* **76**, 2662 (1982).
- ⁵⁶M. Sprik, R. W. Impey, and M. L. Klein, *Phys. Rev. B* **29**, 4368 (1984).
- ⁵⁷M. Born and K. Huang, *Dynamical Theory of Crystal Lattice* (Oxford University Press, London, 1968).
- ⁵⁸A more accurate method to calculate the elastic constants in molecular dynamics has been proposed by J. R. Ray and A. Rahman, *J. Chem. Phys.* **80**, 4423 (1984); J. R. Ray, M. C. Moody, and A. Rahman, *Phys. Rev. B* **32**, 733 (1985); **33**, 895 (1986).
- ⁵⁹*Condensed Matter Research Using Neutrons*, Vol. 112 of *NATO Advanced Study Institute, Series B: Physics*, edited by S. W. Lovesey and R. Scherm (Plenum, New York, 1984).
- ⁶⁰S. Califano, V. Schettino, and N. Neto, *Lattice Dynamics of Molecular Crystals* (Springer, Heidelberg, 1981).
- ⁶¹M. L. Klein, in *Molecular-Dynamics Simulation of Statistical-Mechanical Systems*, edited by G. Ciccotti and W. G. Hoover (North-Holland, Amsterdam, 1986), p. 424.
- ⁶²W. Jin and S. D. Mahanti (unpublished).
- ⁶³D. Sahu and S. D. Mahanti, *Phys. Rev. B* **26**, 2981 (1982); **29**, 340 (1984).
- ⁶⁴S. D. Mahanti, G. Zhang, and G. Kemeny, *Phys. Rev. B* **35**, 8551 (1987).
- ⁶⁵S. W. Lovesey, *Condensed Matter Physics: Dynamic Correlation*, 2nd ed. (Benjamin, New York, 1986).
- ⁶⁶L. Van Hove, *Phys. Rev.* **95**, 249 (1954); **93**, 1374 (1954).
- ⁶⁷T. R. Koehler and P. A. Lee, *J. Comput. Phys.* **22**, 319 (1976).
- ⁶⁸S. Haussühl, *Solid State Commun.* **13**, 147 (1973).
- ⁶⁹A. Loidl, K. Knorr, J. Daubert, W. Dultz, and W. J. Fitzgerald, *Z. Phys. B* **38**, 153 (1980).
- ⁷⁰M. L. Klein and I. R. McDonald, *J. Chem. Phys.* **79**, 2333 (1983).
- ⁷¹A. D. Bruce and R. A. Cowley, *Structural Phase Transition* (Taylor and Francis, London, 1981).
- ⁷²K. H. Michel, *Z. Phys. B* **54**, 129 (1984); K. Żabińska and P. Zieliński, *ibid.* **B 58**, 173 (1985).